2017

Fully Compositional Multi-Scale Reservoir Simulation of Various CO_2 Sequestration Mechanisms

Denis V. Voskov

Heath Henley
University of Rhode Island

Angelo Lucia
University of Rhode Island, alucia@uri.edu

Citation/Publisher Attribution

Voskov, D. V., Henley, H., & Lucia, L. (2017). Fully Compositional Multi-Scale Reservoir Simulation of Various CO_2 Sequestration Mechanisms. *Computers & Chemical Engineering, 96*(4), 183-195. doi: 10.1016/j.compchemeng.2016.09.021
Available at: http://dx.doi.org/10.1016/j.compchemeng.2016.09.021

Fully Compositional Multi-Scale Reservoir Simulation of Various CO_2 Sequestration Mechanisms

Fully Compositional Multi-Scale Reservoir Simulation of Various CO_2 Sequestration Mechanisms

Denis V. Voskov
Delft University of Technology
Department of Geoscience & Engineering
Stevinweg 1, 2628 CN Delft, NL

Heath Henley & Angelo Lucia*
Department of Chemical Engineering
University of Rhode Island
Kingston, RI 02882 USA

* Corresponding author: Tel: +1 401 874-2814; Email: alucia@uri.edu

Abstract

A multi-scale reservoir simulation framework for large-scale, multiphase flow with mineral precipitation in CO_2-brine systems is proposed. The novel aspects of this reservoir modeling and simulation framework are centered around the seminal coupling of rigorous reactive transport with full compositional modeling and consist of (1) thermal, multi-phase flow tightly coupled to complex phase behavior, (2) the use of the Gibbs-Helmholtz Constrained (GHC) equation of state, (3) the presence of multiple homogeneous/heterogeneous chemical reactions, (4) the inclusion of mineral precipitation/dissolution, and (5) the presence of homogeneous/heterogeneous formations. The proposed modeling and simulation framework is implemented using the ADGPRS/GFLASH system. A number of examples relevant to CO_2 sequestration including salt precipitation and solubility/mineral trapping are presented and geometric illustrations are used to elucidate key attributes of the proposed modeling framework.

Keywords: mineral deposition/dissolution, carbon sequestration, Gibbs-Helmholtz constrained equation of state, numerical reservoir simulation

1. Introduction

1.0 Background and motivation

Atmospheric carbon dioxide emission has become a growing concern for the scientific community over recent decades. As a result, interest in methods of carbon capture and storage (CCS) have grown, including gas injection for enhanced oil recovery (EOR), recycling for industrial uses (Lueng et al., 2014), and storage in geological formations (e.g., in depleted oil reservoirs, unminable coal beds and saline aquifers), the last of which is generally considered the most viable method (Lueng et al., 2014; Bachu & Adams, 2003; Celia & Nordbotten, 2009; van der Zwaan & Smekens, 2009) for the storage of large amounts of carbon dioxide.

Thermal multiphase flow and compositional reactive transport in porous media is the basis for simulation of almost all energy and environment-related industrial processes. The development of a simulation framework capable of modeling this class of problems on a continuous scale has been an important task in both the reservoir engineering and hydrology communities. Reservoir engineers usually deal with problems involving thermal multiphase flow and multi-component transport tightly coupled with complex phase behavior (Zaydullin et al., 2014). These problems include different enhanced oil recovery processes such as steam or gas injection. Usually, chemical reactions are not treated as having a first-order impact on these models.

On the other hand, the hydrology community has been concerned with subsurface modeling of multiple components and multiple chemical reactions. The work by Lichtner (1985) laid the theoretical foundation for continuum models for mass transport and chemical interactions. Current chemical models include a wide variety of different reactions, including dissolution-precipitation and adsorption-desorption (Steefel et al., 2005). However, these models mostly deal with only the aqueous phase in slightly heterogeneous reservoirs. Reactive transport modeling in subsurface hydrology has never been fully coupled with equilibrium phase behavior of complex hydrocarbon mixtures in highly heterogeneous formations, despite some recent attempts (Flemisch et al., 2011). Due to the emerging interest in complicated subsurface dynamic processes like CO_2 sequestration, methane hydrate recovery, and geothermal processes, there is a growing need in integrating full chemical reaction modeling capabilities with compositional reservoir simulation (Marchand and Knabner, 2014; Farshidi, 2016). Any heterogeneous structure of subsurface formations and the multiple scales of governing processes requires implicit time approximation for numerical solutions to be unconditionally stable on simulation time-steps appropriate for the problem of interest.

The main purpose of this study was to develop, for the first time, capabilities for reactive transport modeling in subsurface hydrology fully coupled to equilibrium phase behavior of complex mixtures in highly heterogeneous formations within a numerical reservoir simulator. We tested our framework on a problem of particular practical importance - CO_2 sequestration in aqueous aquifers. One of the major challenges in modeling this class of problems is accurate representation of dissolution trapping (Elenius et al. 2014, 2015). Macroscopic dissolution rates can be enhanced significantly by gravity-driven currents (up to an order of magnitude). This complex behavior is strongly affected by many factors, including the chemical composition of the brine, different impurities in the injection stream of CO_2, changes in

pressure and temperature, and simultaneous chemical reactions. In addition, small scale precipitation and dissolution of minerals impacts the dynamics of gravity-driven flows and, in turn, effects the dissolution as well. This work is the first attempt to create a universal tool for predictive reservoir simulation of CO_2 sequestration in aqueous aquifers that takes into account all of the complex mechanisms that effect the macroscopic dissolution rate. This dissolution rate can then be used in a realistic, large-scale reservoir model using simplified physical models (Gasda et al., 2011; Lagasca, 2014) to predict the dynamic of CO_2 trapping for medium time scales (i.e., tens to a hundred thousand years).

Accordingly, the remainder of this article is organized as follows. Sections 1.1 and 1.2 present an overview of the current literature for numerical reservoir simulation and EOS modeling of CCS systems, respectively. Section 2 describes the formulation of the fully coupled, multi-phase flow/chemical/phase equilibrium equations as well as the GHC equation of state within the software libraries used in this work (ADGPRS and GFLASH). Attributes of the basic numerical reservoir modeling such as fully compositional, model equations, grid generation, etc. and the key features of the phase/chemical equilibrium modeled by the GHC equation (i.e., the GHC expression for the energy parameter, incorporation of molecular information from Monte Carlo simulation, chemical equilibrium modeling, etc.) are needed to understand the details of the CO_2 sequestration applications studied in this work. Results for several examples illustrating mineral dissolution/deposition and/or mineral trapping in CO_2 sequestration processes are presented and discussed in detail in Section 3. From the results of this study, conclusions are drawn and described in Section 4.

1.1 Numerical reservoir simulation

Most nonlinear formulations can be described as either phase based (e.g. natural formulation, Coats, 1980), or mass based (e.g. molar formulation, Acs et al., 1985). Both of these formulations have their advantages and drawbacks (Voskov and Tchelepi, 2012). For multiphase multi-component flow and transport, the natural formulation helps to control the nonlinearities in fluxes. However, it requires a robust implementation of variable substitution techniques (Voskov, 2011). Also, in natural variables, only approximate masses for each component can be evaluated on any nonlinear iteration until convergence to the solution is reached and this introduces challenges for efficient coupling with chemical reactions (Farshidi, 2016). In the molar formulation, on the other hand, the mass of each component is known exactly on each nonlinear iteration, which makes it more appropriate for reactive transport. However, the nonlinearities in fluxes are often poorly resolved in the molar formulation and that requires designing better nonlinear solvers (Voskov and Tchelepi, 2012).

Recently, several nonlinear formulations were proposed based on an adaptation of the negative flash for natural formulation (Abadpour and Panfilov, 2009) and a complementary condition for thermodynamic equilibrium (Lauser et al., 2011). These approaches were designed to improve the nonlinear behavior associated with multiphase changes. The idea described in (Abadpour and Panfilov, 2009) was extended for general purpose simulation and tested against state of the art approaches (Voskov, 2012). For problems of practical interest, the performance of the extended natural formulation shows only insignificant and case-dependent improvements when compared with the classic natural formulation. The natural formulation with the complimentary condition was studied for compositional

problems of practical interest in Gharbia et al. (2015) and showed that the conventional natural formulation outperforms the natural formulation with a complimentary condition. In this paper we present an extension of the natural formulation for equilibrium chemical reactions including precipitation and dissolution of minerals.

1.2 EOS modeling

Additional complexity in compositional modeling stems from phase behavior computations. An Equation of State (EoS) model is usually employed to describe the phase behavior of multi-component system (Lake, 1989). For a given temperature, pressure, and overall composition, EoS computations define the phase state and composition of each phase (Michelsen, 1982a,b). Since iterative EoS computations must be performed for each computational cell and for each global nonlinear iteration, they can constitute a significant fraction of the total computational cost, even though several schemes exist to speed up these computations in the natural formulation (Rasmussen et al., 2006; Voskov and Tchelepi, 2009; Pan and Tchelepi, 2011; Zaydullin et al., 2016).

Another challenge is related to the accuracy of the EoS for systems involving simultaneous phase and chemical equilibrium for homogeneous and heterogeneous chemical reactions. There are no journal articles in the open literature that consider all of these problems attributes together. Many models use correlations instead of rigorous EoS computations to determine fluid properties and equilibrium. For example, the fluid property module, ECO2N (Pruess and Spycher, 2007) was specifically designed for geological CO_2 sequestration in conjunction with the TOUGH2 reservoir simulator. This model considers the simple system of NaCl-CO_2-water and (1) treats the CO_2 phase as a pure phase and uses tabulated correlation instead of an EoS for the CO_2 molar volume, (2) uses a temperature correlation to determine whether NaCl precipitates or not, which ignores the presence of CO_2, and (3) does not take into account the reaction of CO_2 + H_2O to form either carbonate or bicarbonate ions or the presence of Ca+ ions.

Most successful thermodynamic models are either activity coefficient models (e.g. NRTL, UNIQUAC or EOS models [Redlich-Kwong (RK) equation (Redlich and Kwong, 1949), Soave-Redlich-Kwong (SRK) equation (Soave, 1972), Peng-Robinson (PR) equation (Peng and Robinson, 1976), Statistical Associating Fluid Theory (SAFT), Huang and Radosz, 1990, Cubic Plus Association (CPA), Kontogeorgis et al., 1996, etc.] and are not directly applicable to aqueous electrolyte system. However, thermodynamic models have also been developed for electrolyte solutions (see Prausnitz, et al. 1999) including Pitzer equations (Pitzer, 1977), the electrolyte NRTL equation (Chen & Song, 2005), the electrolyte Predictive SRK (ePSRK) equation (Kiepe et al., 2005), the GHC equation (Lucia et al., 2014), the eCPA equation (Moribo-Mogensen et al., 2015), and variants of Statistical Associating Fluid Theory or SAFT (Chapman et al., 1990). Unfortunately, many of the rigorous EoS models such as the recent modifications for the activity coefficient part of the ePSRK model, LIQUAC/LIFAC, by Mohs and Gmehling (2013) mention salt precipitation but present no results illustrating capabilities and do not consider simultaneous homogeneous chemical reaction. The electrolyte Cubic Plus Association (eCPA) model of Maribo-Mogensen et al. (2015), on the other hand, only considers phase equilibrium of electrolyte mixtures and no chemical reactions. Finally, the recent electrolyte version of SAFT (Zhao et al., 2007) does not consider solid precipitation either.

2. Modeling

In this section, the GHC EOS and numerical reservoir simulator, ADGPRS, are briefly discussed and advantages of each are highlighted.

2.1 GHC equation of state

The GHC EOS (Lucia, 2010) is a recent modification of the SRK (Soave, 1972) EOS that constrains the energy parameter, a, to satisfy the Gibbs-Helmholtz equation and uses Monte Carlo simulations to incorporate molecular length scale information. In particular, the energy parameter in the GHC EOS for pure components is given by equation (1).

$$a(T,p) = \left(0.42748 * \frac{R^2 T_c}{p_c} + \frac{bU^{DL}}{T_c \ln(2)} + \frac{2bR ln(T_c)}{\ln(2)}\right) T - \frac{bU^{DL}}{\ln(2)} - \left(\frac{2bR}{\ln(2)}\right) T ln(T) \quad (1)$$

where p_c and T_c are critical properties, b is the molecular co-volume parameter, and R is the gas constant, and U^D is the molecular scale internal energy of departure at the given temperature and pressure. Pure component U^D is determined *a priori* over wide ranges of temperature and pressure using Monte Carlo molecular simulation, stored in look up tables, and readily up-scaled to bulk phase EOS calculations using Eq. (1). The novel features of the GHC equation include the use of molecular information in the energy parameter expression and the estimation of b from pure component density data. The details of the derivation of the GHC EOS, the extension to non-electrolyte and electrolyte mixtures can be found in the literature (Lucia, 2010; Lucia et al., 2012a, b; Lucia et al., 2015). It is important to note that the GHC EOS only uses parameters based on pure component properties (e.g., mixture critical properties from Kay's rules) and pure component Monte Carlo molecular simulation (mixture internal energies of departure, U_M^D, are computed from a linear mixing rule), even in systems containing electrolytes, and is truly predictive.

2.1.2 Monte Carlo simulation details

Application of the multi-scale GHC EOS requires prior knowledge of pure component internal energy of departure for the components in the system at relevant conditions. Monte Carlo molecular simulations in the isobaric-isothermal ensemble are used to generate the necessary information *a priori* and create lookup tables. The specific details of the simulation change based on the component and molecular model being used, however generally a 6-12 Lennard-Jones potential is used to account for van der Waals interactions, along with the recommended cut off (depending on the model) and tail corrections. The Coulomb potential with an Ewald summation is used to account for electrostatic interactions. A cubic box with periodic boundary conditions is used in all bulk fluid simulations. Standard center of mass translation and rotation moves, as well as isotropic volume moves are applied. Simulations are run in equilibration mode for a number of cycles (depending on the system) in which the maximum displacement and rotation are frequently adjusted to maintain 50% acceptance rates of translation and rotation moves, respectively. The system is then switched to production mode, in which the maximum displacement and rotation are fixed, for sampling. Typically, four parallel sets are run for the same system and the results are averaged. References for the simulation parameters for the components used in this work can be found Table B.3.

Simulations are typically run either using either the open source Towhee MCCCS software (Martin, 2013) or an in-house FORTRAN program. MC simulation runtimes can range from a few hours to a few days, depending on the complexity of the molecular model, the number of particles included in the simulation, and the potential model(s) used.

2.2 GFLASH

The GFLASH library is a multi-component, multiphase, isothermal, isobaric (TP) flash calculation program written in FORTRAN. Given an overall composition, temperature, and pressure of a fluid mixture, GFLASH has the capability to calculate existing phases at equilibrium, their compositions, densities, enthalpies, fugacities, and all property derivatives with respect to pressure, temperature, and composition. The main capabilities and details are outlined in previous publications (Zaydullin et al., 2014; Lucia, et al., 2015). The main reasons for the use of GFLASH in this work are the implementation of (1) a robust stability and flash algorithm and (2) the GHC EOS, and (3) the capability to handle simultaneous phase and homogeneous/heterogeneous chemical reaction equilibrium with mineral deposition/dissolution.

2.2.1 Description of chemical reaction equilibrium model

A full detailed description of the numerical methods used for solving the equilibrium reactions for molecular salt formation included in this work can be found in the paper by Lucia et al. (2014). For the examples studied in this work, the formation/dissolution of solid salts was limited to NaCl, Na_2CO_3, $CaCl_2$, and $CaCO_3$, described by the following reactions:

$$NaCl_{(s)} \leftrightarrow Na^{+}_{(aq)} + Cl^{-}_{(aq)} \quad (2)$$

$$Na_2CO_{3(s)} \leftrightarrow 2Na^{+}_{(aq)} + CO^{2-}_{3(aq)} \quad (3)$$

$$CaCl_{2(s)} \leftrightarrow Ca^{2+}_{(aq)} + Cl^{-}_{(aq)} \quad (4)$$

$$CaCO_{3(s)} \leftrightarrow Ca^{2+}_{(aq)} + CO^{2-}_{3\ (aq)} \quad (5)$$

In addition, the following reaction of dissolved carbon dioxide with water to generate carbonate ion was included:

$$CO_2 + 3H_2O \leftrightarrow 2H_3O^{+}_{(aq)} + CO^{2-}_{3(aq)} \quad (6)$$

Reaction (6) was obtained by summing the reactions in the carbonate series, and equilibrium concentrations of carbonic acid and bicarbonate ion, which were not of interest in the examples studied. Also, the formation of hydronium ion, and therefore changes in pH due to the dissolution of CO_2, were neglected. This is because Soong and coworkers (2004) have found that brine with a pH of 11 produces the most $CaCO_3$ when reacted with CO_2. Therefore, it is assumed that the original pH of formation brine was high enough to fully support $CaCO_3$ precipitation. For a brine solution with pH of 11, the change in pH due to the amount of CO_3^{2-} produced from CO_2 in the examples in this study was, in fact, negligible, as shown in Appendix A. The equilibrium constants for the reactions were calculated from tabulated

standard Gibbs free energies of formation data and corrected for temperature using tabulated standard enthalpies of formation and the van't Hoff equation. See Appendix B.

The primary goals of this study were (1) to demonstrate that the coupled ADGPRS/GFLASH software system has the capability to accurately model mixtures in which minerals dissolve and/or precipitate and (2) to show that ADGPRS/GFLASH can accurately model CO_2 sequestration with residual, dissolution, and mineral trapping.

2.3 ADGPRS

The reservoir modeling software used in this work is called Automatic Differentiation General Purpose Research Simulator (ADGPRS) and was developed and maintained by SUPRI-B research group at Stanford University. ADGPRS is written mainly in C++, and widely used throughout the reservoir and petroleum engineering communities because of its wide ranging capabilities, which include (Zaydullin et al., 2014):

1. Flexible treatment of all nonlinear physics.
2. A fully thermal-compositional formulation for any number of phases.
3. Multi-phase CSAT for efficient and robust computation of phase behavior.
4. A variety of spatial and temporal discretization schemes.
5. Thermal geo-mechanical modeling including the effects of fractures.
6. A fully coupled, thermal, multi-segmented well model with drift-flux.
7. An adjoint-based optimization module.

The details of ADGPRS, including (1) available variable formulations (Voskov & Tchelepi, 2012; Zaydullin et al., 2012), (2) discretization schemes (Zhou et al., 2012), (3) solution methods for the system of linear and nonlinear equations (Voskov, 2011; Tchelepi & Zhou, 2013), and (4) various approaches for phase behavior computations (Iranshahr et al., 2010 and 2013) can be found in the literature cited. An overview of the topics previously listed is given in a previous paper (Zaydullin et al., 2014) and is not included here.

2.4 Coupling ADGPRS/GFLASH for compositional systems

Interfacing GFLASH with ADGPRS results in a fully implicit and fully coupled treatment of the flow and transport through porous media, as well as rigorous, EOS-based phase/chemical equilibrium. GFLASH determines the equilibrium compositions of all phases using rigorous Gibbs free energy minimization along with the density of the fluid phases and provides accurate densities for the fluid phases without the need for empirical correlations such as volume translation and binary interaction parameters. ADGPRS/GFLASH has been successfully used to compare different enhanced oil recovery (EOR) methods in both light and heavy oil reservoirs. The details of the interface can be found in the literature (Zaydullin et al., 2014, Voskov et al., 2016).

2.4.1 ADGPRS/GFLASH architecture

Figure 1 clearly illustrates the architecture of the ADGPRS/GFLASH modeling framework, with a focus on the flow of information in the GFLASH library.

Fluid densities and fugacities, as well as chemical reaction equilibrium constraints and their derivatives for the fluids in each grid block in the reservoir model, are calculated at given conditions (temperature, pressure and composition) and returned to the simulator. As described in section 2.1, the molecular level information required to use the GHC equation of state is obtained *a priori* and stored in pure component look-up tables for the components of interest. To perform EOS based calculations the U^D s for all components in the mixture are read from the look-up tables and, if necessary, interpolated to the conditions of interest. It is important to note the GHC EOS requires no adjustable parameters at the EOS level. Critical properties for all components used in this work are listed in B.1, as well as the values of the molecular co-volumes for the GHC EOS. See Lucia et al. (2012) and Lucia et al. (2014) respectively for additional information regarding the implementation of the GHC EOS and the multiphase flash algorithm and handling of salt precipitation within GFLASH.

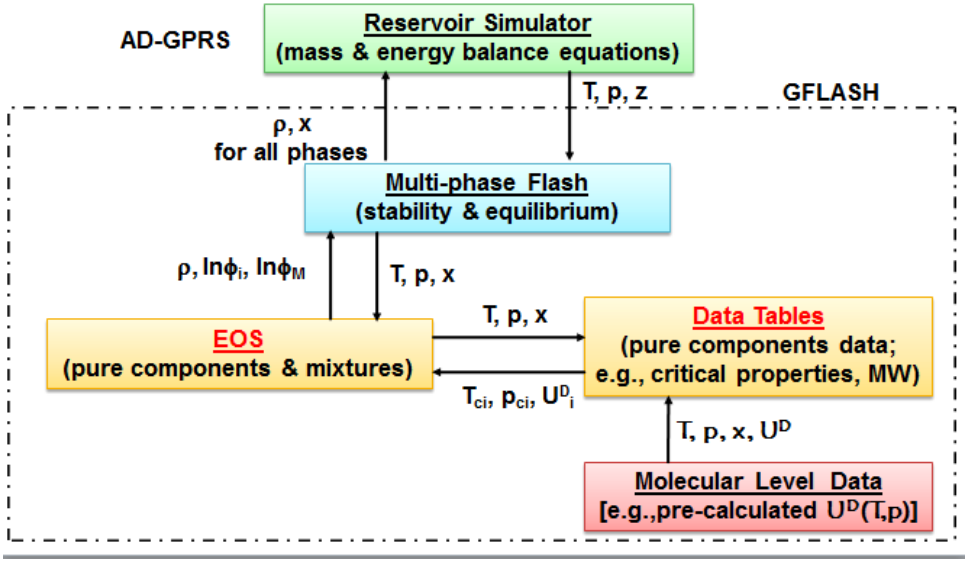

Figure 1: Schematic Diagram Illustrating Information Flow in ADGPRS/GFLASH Framework

3. Natural Formulation for Reactive Systems with Precipitation and Dissolution

The basic information flow between ADGPRS and GFLASH is given in Fig. 1. Specifically, for each grid block in the reservoir ADGPRS passes the current estimate of the temperature, pressure and overall composition of that block to GFLASH. GFLASH, in turn, uses that information to determine the number of equilibrium phases, their amounts and compositions, in this case using the GHC equation of state, and returns this information to ADGPRS. Many of these details are described in previous publications (Zaydullin et al., 2014; Voskov et al., 2016). In this section, specific modifications for the treatment of flow and transport in the presence of chemical (equilibrium) reactions are described and details of the coupling between ADGPRS and GFLASH was extended. For problems with precipitation and dissolution with equilibrium reactions, new (solid) phases must be introduced into the general natural variables logic (Voskov and Tchelepi, 2012; Zaydullin et al. 2014).

3.1 Governing equations

The typical governing equations for CO_2 sequestration include conservation of mass for each species and closure assumptions and constraints. The mass conservation equations for isothermal compositional systems can be written as

$$\frac{\partial}{\partial t}\left(\phi \sum_{k=1}^{P} \rho^k x_i^k S^k\right) - \sum_{k=1}^{P} \nabla\left(\rho^k x_i^k \mathbf{V^k} + S^k \mathbf{J_i^k}\right) - q_i = \sum_{l=1}^{R} r^l v_i^l, \; i = 1, \ldots, C \tag{7}$$

where P is the number of co-existing thermodynamic phases, R is the number of reactions, and C is the number of species. Also, ϕ is the porosity of the porous media, ρ is molar density, x denotes composition in mole fraction, S is phase saturation, $\mathbf{V}$ is volumetric (Darcy) flow, $\mathbf{J}$ is molar diffusion flux, q denotes a mass source or sink term, r is reaction rate, and v are stoichiometric coefficients.

3.2 Rearrangement of equations

Equation (7) can be written in the general matrix form given by

$$\frac{\partial \mathbf{a}}{\partial t} + \mathbf{l} + \mathbf{q} = \mathbf{V}\mathbf{r} \tag{8}$$

where **a** corresponds to an accumulation vector of length C, **l** is a C vector of fluxes, **q** is the well source term vector, also of length C, **r** is the reaction rate vector of length Q, and **V** is a $C \; x \; Q$ stoichiometric matrix.

Following the logic described in Farshidi et al. (2013), we introduce the $E \; x \; C$ matrix, **E**, which represents the stoichiometry for each element associated with the reactions of each species. In general, this matrix can be determined by solving the equations

$$\mathbf{E} \times \mathbf{V} = \mathbf{0} \tag{9}$$

Multiplying Eq. (8) by **E** gives E element mass conservation equations of the form

$$\frac{\partial \mathbf{E}\mathbf{a}}{\partial t} + \mathbf{E}\mathbf{l} + \mathbf{E}\mathbf{q} = \mathbf{0} \tag{10}$$

To close the system, an additional $C - E$ independent equilibrium constraints are needed and take the form

$$K_{sp}(T, p) - Q_{sp}(\boldsymbol{x}, p, T) = 0 \tag{11}$$

where the multi-phase flash procedure described in Section 2.2 is used to define the equilibrium solubility product, $K_{sp}(p, T)$, using Gibbs free energies of formation and the identity of the minerals that precipitate. The ion solubility product, $Q_{sp}(\boldsymbol{x}, T, p)$, on the other hand, is defined using the actual ion concentrations in the brine determined from the GHC equation of state.

3.3 Mineral precipitation

When mineral precipitation is controlled by chemical equilibrium, a procedure is needed to account for the appearance and/or disappearance of solids. Since precipitation only occurs when the ion solubility product for any particular salt exceeds its equilibrium solubility product, a more general form of Eq. (10)

is needed.

$$Q_{sp}(\boldsymbol{x}, T, p) > K_{sp}(p, T); \text{ precipitation}$$
$$Q_{sp}(\boldsymbol{x}, T, p) \leq K_{sp}(p, T); \text{ no precipitation} \quad (12)$$

Once the potential for precipitation is identified, new conservation equations for those mineral components and mineral phases of the form

$$\frac{\partial \mathbf{a_c}}{\partial t} = \mathbf{r_c} \quad (13)$$

must be added to the original system given in Eq. (8). Additional unknown variables must also be added to the set of unknowns corresponding to the concentrations of the solid species. Finally, the matrix E should be modified and include a new rate corresponding to the reaction for the precipitated mineral, see Farshidi (2016) for details.

3.4 Illustrative example

In this section, a simple example is presented to illustrate the extension of the compositional AD-GPRS/GFLASH framework to reactive systems with five components and three phases as shown in Table 1 .

Table 1: Presence of Components in Phases

Phase/Components	H_2O	CO_2	Ca^{2+}	CO^{2-}	$CaCO_3$
1. Brine	x	x	X	x	-
2. Gas	x	x	-	-	-
3. Mineral	-	-	-	-	x

For simplicity, we assume that the brine phase always exists. Treatment of the disappearance of water or brine phases can be found in Farshidi (2016). For the illustrative example, there are only four possible combinations of co-existing phases, as shown in Table 2.

Table 2: Status Table and Equations for Brine-CO_2 System

Status	Number of phases	Array of existing phases		
		Brine	Gas	Solid
1	1	X	-	-
2	2	X	x	-
3	2	X	-	x
4	3	X	x	x

The matrix **E** for this example is

$$\boldsymbol{E} = \begin{bmatrix} 1 & 0 & 0 & 0 \\ 0 & 1 & 0 & 0 \\ 0 & 0 & 1 & 0 \\ 0 & 0 & 0 & 1 \end{bmatrix} \tag{14}$$

when solid phase does not precipitate and

$$\boldsymbol{E} = \begin{bmatrix} 1 & 0 & 0 & 0 & 0 \\ 0 & 1 & 0 & 0 & 0 \\ 0 & 0 & 1 & 0 & 1 \\ 0 & 0 & 0 & 1 & 1 \end{bmatrix} \tag{15}$$

when solid precipitates and correspond to statuses 3 and 4. For the matrices shown in Eqs. (14) and (15), each row corresponds to an element (i.e., carbon, hydrogen, oxygen, etc.) while each column corresponds to a component (i.e., molecular or ionic species). Finally, a correct set of unknowns (and equations) can be easily constructed for each combination of phases shown in Table 2.

4. Numerical Results and Discussion

In this section, numerical results for four separate CO_2 sequestration examples are presented to illustrate the robustness of the proposed methodology in capturing the correct physics of solubility and mineral trapping, carbonate chemistry, and mineral precipitation and dissolution.

Example 1 - Large Scale Model with Solid Precipitation and Dissolution

This first example is a simple reservoir model with the fluid system of CO_2-H_2O-Ca^{2+}-Na^{+}-Cl^{-}-CO_3^{2-}. For the conditions shown in Table 3, there are many different equilibrium phase states possible (i.e., VLE, VLLE, LLE, SLE, SLLE, etc.), depending on temperature, pressure and composition throughout the reservoir. The main purpose of this example was to demonstrate the ability of the ADGPRS/GFLASH system to model solid precipitation and dissolution; therefore carbonate chemistry was not included and represents a system in which a CO_2-rich injection stream is introduced into a formation containing a single phase brine. It is set up in a 50x50x1 grid to study horizontal propagation of the injection stream.

As shown in Table 3, the injection feed contained an elevated carbonate composition due to higher carbon dioxide composition. Transmissibility in both the x and y directions was set to 10.0. A formation porosity of 0.18 was used and simulations were conducted isothermally (energy balance neglected) at a temperature of 350 K. In addition, the GHC EOS was used to evaluate all densities, fugacities, and required derivatives and all salt equilibrium and ion solubility calculations were performed by GFLASH. A natural variable formulation, in which pressure, saturations, and component phase compositions were the independent variables, was used for the simulations using ADGPRS.

This particular example contained an injection well in the lower left corner, and a production well in the upper right hand corner. As shown in Table 3, the reservoir was initialized with solid NaCl in each block and a fluid with a composition different than composition of the injected fluid.

Table 3: Initial Conditions for 50x50x1 Example

	Injection conditions	Reservoir
Quantity	**Value**	**Value**
p (bar), T (K)	**240, 350**	**220, 350**
Species	**Mole Fraction**	**Mole Fraction**
CO_2	0.979997	0.000500
H_2O	0.020000	0.994300
Na^+	0.000002	0.002000
Ca^{2+}	1.00E-13	0.000400
Cl^-	1.00E-13	0.002800
CO_3^{2-}	0.000001	1.000000E-13
Minerals	**Concentration (kmol/m^3)**	**Concentration (kmol/m^3)**
NaCl	0	1.2
$CaCl_2$	0	0
Na_2CO_3	0	0
$CaCO_3$	0	0

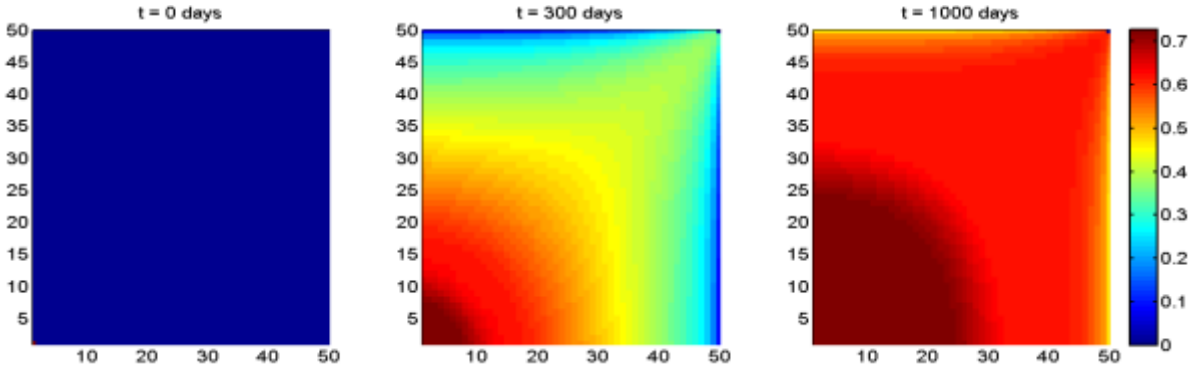

Figure 2: CO_2-rich Phase Saturation Distribution

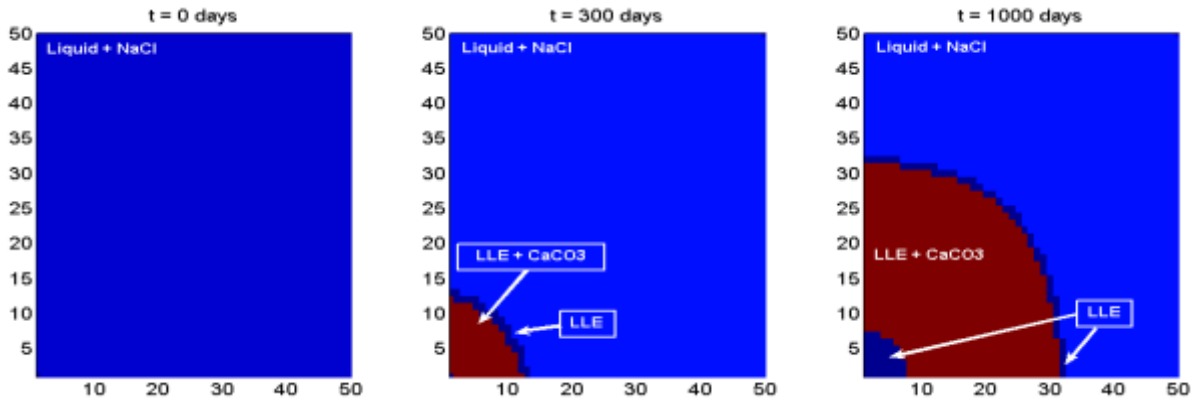

Figure 3: Equilibrium Phase State Distribution

As the simulation of this first example progressed, the pressure changed until supercritical CO_2 broke into the production well in the upper right hand corner. Also, the flow of CO_2 from the injection block caused an increase in CO_2 composition in many blocks of the reservoir, eventually causing a second CO_2 rich phase to appear in the system (see figure 2). Figure 3, on the other hand, shows the equilibrium phase state (i.e., LLE, SLLE, VLE, etc.) of each block in the system as the simulation evolved. Clearly, Fig. 3 shows that as fluid flowed out of the feed block into the reservoir, NaCl dissolved before the Ca^{2+} in the reservoir could react with CO_3^{2+} from the feed block to form $CaCO_3$.

This example clearly illustrates the capabilities of the ADGPRS/GFLASH system to model both mineral dissolution (NaCl) and precipitation ($CaCO_3$) using a rigorous EOS-based treatment of the phase equilibrium. Some current reservoir simulation frameworks rely on tabulated K-values (e.g., CMG STARS) while others, like the ECO2N module (Pruess and Spycher, 2007) in the TOUGH2 simulator, use correlations to determine the vapor-liquid equilibrium instead of a rigorous EOS-based flash calculation.

Example 2 –Large Scale simulation of CO_2 Injection

The purpose of this second example was to demonstrate that the coupled ADGPRS/GFLASH system could successfully model $CaCO_3$ precipitation/dissolution. This second example focused on buoyancy driven vertical migration of a CO_2 plume, which is a key feature of many carbon sequestration studies, the use of approximate carbonate chemistry, and its impact on the precipitation of $CaCO_3$ as described in section 2.2.1. Here we assume that the CO_2 plume is trapped in the geological formation and monitor short time-scale mineralization processes. This example used the same fluid system that was used in example 1 with conditions shown in Table 4. More specifically, the reservoir in this example was homogeneous with a porosity of 0.18 and discretized with a 25x1x25 grid. The grid spacing was also homogeneous and set to 8 m in each direction, with absolute permeability equal to 150 mD and 220 mD in the x and z directions respectively. This system was first equilibrated to approximate hydrostatic equilibrium so that the pressure in the initial system varied with depth from 250 bars to 270 bars. Pure CO_2, which was less dense than the surrounding reservoir fluid, was injected into the middle block in the bottom row of the reservoir. The increased amount of CO_2 that dissolved in reservoir brine resulted in an increase in dissolved carbonate ions in the aqueous phase, and under the model conditions defined in this example, also resulted in the precipitation of $CaCO_3$. As this CO_2 plume rose, it was observed that

the amount of dissolved CO_2 in the aqueous phase in the blocks near the plum increased. This, in turn, led to the generation of CO_3^{2-}, which then reacted with dissolved Ca^{2+} in the reservoir to form solid $CaCO_3$.

Table 4: Initial Conditions for a 25x1x25 Example

	Injection conditions	Reservoir
Quantity	**Value**	**Value**
p (bar), T (K)	**280, 350**	**250-270, 350**
Species	**Mole Fraction**	**Mole Fraction**
CO_2	0.430000	1.0000e-5
H_2O	0.569979	0.999689
Na^+	1.0000e-13	1.0000e-13
Ca^{2+}	1.0000e-13	1.0000e-4
Cl^-	1.0000e-13	2.0000e-4
CO_3^{2-}	1.0000e-13	1.0000e-13
Mineral	**Concentration (kmol/m^3)**	**Concentration (kmol/m^3)**
NaCl	0.0	0.0
$CaCl_2$	0.0	0.0
Na_2CO_3	0.0	0.0
$CaCO_3$	0.0	0.0

Figure 4 shows the CO_2-rich phase saturation at selected time steps, while Figs. 5 and 6 show the concentration of CO_2 in the brine phase and amount of precipitated $CaCO_3$ respectively.

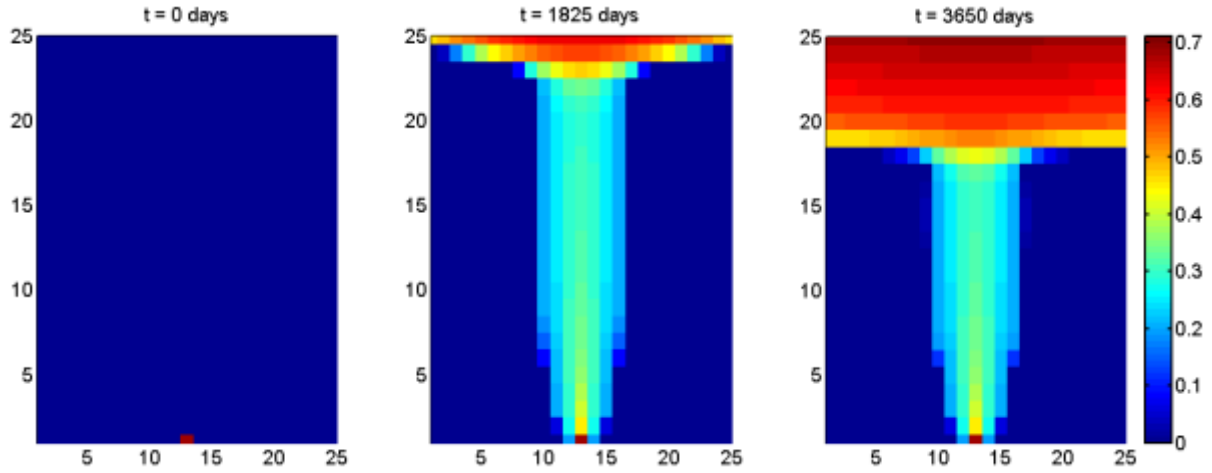

Figure 4: CO_2-Rich Phase Saturation Distribution

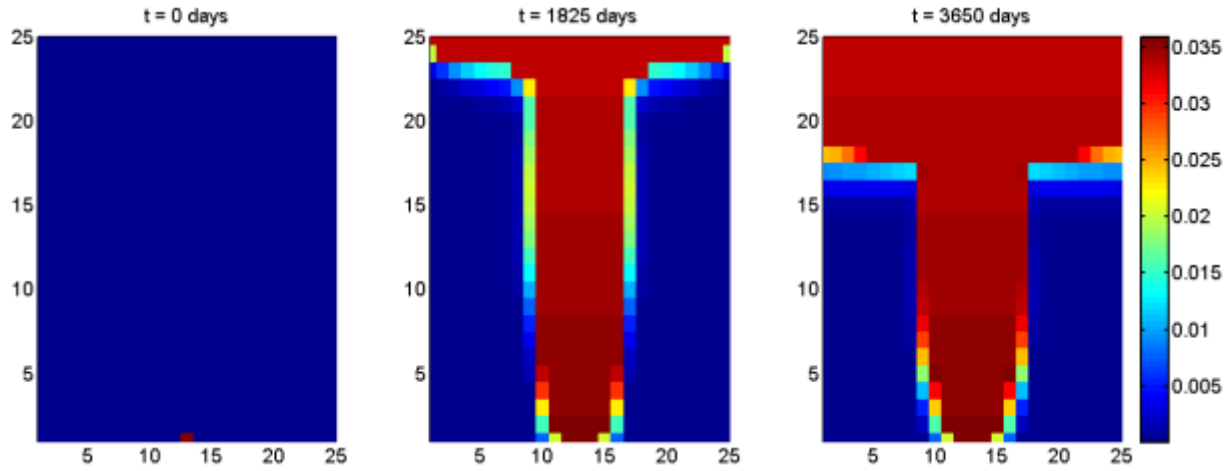

Figure 5: Distribution of CO_2 Mole Fraction in the Brine Phase

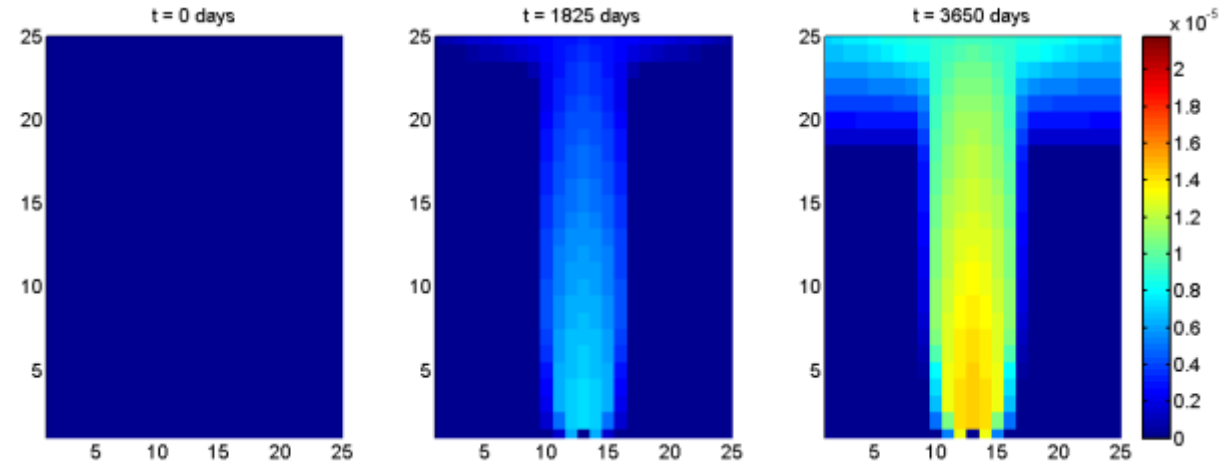

Figure 6: Distribution of Precipitated $CaCO_3$ (kmol/m^3)

It is clear from Figs. 4-6 that the CO_2 plume migrates upward, causing an increase dissolved CO_2 in the brine phase, leading to precipitation of $CaCO_3$. Moreover, in this example the only source of CO_3^{2-} ions was the equilibrium reaction between dissolved carbon dioxide and water and the resulting precipitation of $CaCO_3$ in the reservoir clearly illustrates that the coupled ADGPRS/GFLASH system has the capability to model salt precipitation in the presence of carbonate chemistry.

Example 3 – Small Scale Model with Solubility Trapping

In this section, we use a simulation model from Elenius et al. (2015) to estimate the small-scale dissolution rate of CO_2. The rectangular 2D domain has dimensions 100 × 50 m with resolution $\Delta x = \Delta z =$ 0.5 m, constant porosity $\phi = 0.15$ and permeability k = 100 mDarcy. There are no flow boundary conditions on the top and sides of the domain and an open downward boundary with a low permeability (k_b = 0.1 mDarcy). This model represents the trailing part of a large-scale plume with a capillary transient zone and the diffusion of dissolved CO_2 through the bedrock. Here instead of using the simplified correlations for properties of CO_2 and brine as was done in Elenius et al. (2015), we used the GHC EoS for property evaluation at different thermodynamic conditions to account for the presence of aqueous

ions. Table 5 gives the initial compositions for the model. We used an initial pressure distribution starting from p = 240 bars at the lower part of the model and constant temperature T = 345 K. No minerals initially precipitated in the model.

Table 5: Initial Composition in Lower Region for Example 3

Component	Mole fraction in lower region (single phase)
CO_2	1.00E-09
H_2O	0.999500148999
Na^+	1.00E-04
Ca^{2+}	1.00E-04
Cl^-	3.00E-04
CO_3^{2-}	1.00E-12

Due to molecular diffusion, the initial portion of CO_2 in the plum starts dissolving in the brine, and the difference in density of the brine with the dissolved CO_2 (since it is heavier than the original brine) initiates the formation of unstable fingers of CO_2-rich brine. These fingers enhance the dissolution rate of CO_2 several fold and significantly increase the trapping capability of the aquifer due to the higher dissolution. The numerical simulation of this process requires very fine resolution of the simulation grid which makes it prohibitive for a full field simulation (Elenius et al., 2015). Small scale models can predict CO_2 dissolution rate quite accurately, which can be used in various up-scaling models (Gasda et al., 2011; Lagasca, 2014) to predict the migration distance of the CO_2 plume in a large aquifer over medium time-scale (tens to one hundred thousand years). The left part of Fig. 7 shows the composition of CO_2 in the brine phase at different times. In the right part of Fig. 7 is shown the dissolution rate of CO_2 as a function of time (years). The dissolution rate and trend are similar to ones reported in Elenius et al. (2015).

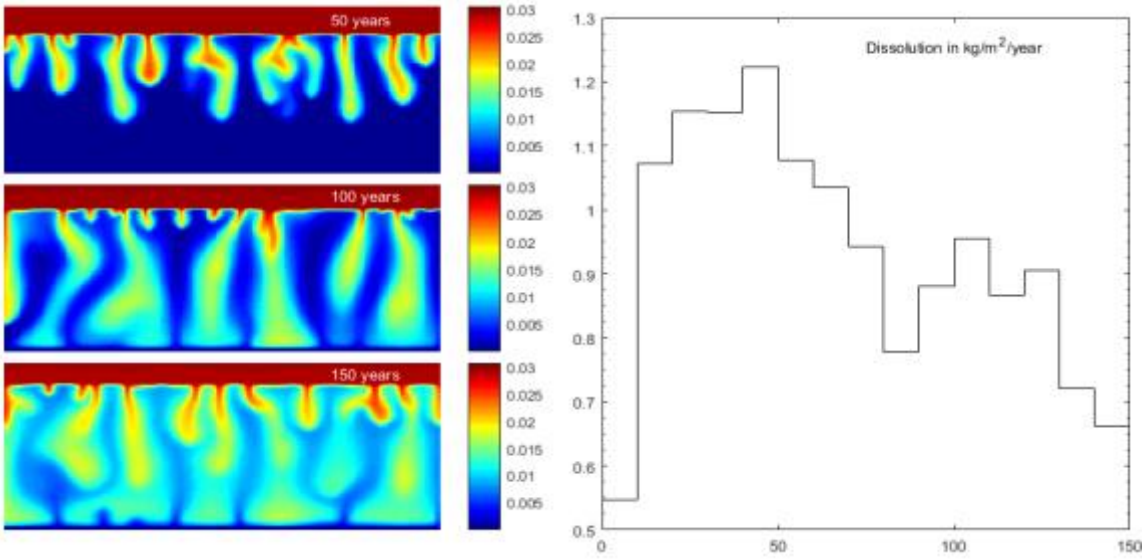

Figure 7: Distribution of CO_2 in Brine at Different Times and Macroscopic Dissolution Rate of CO_2 as a Function of Time for Simulation at T = 345 K

Example 4 – Small Scale Model with Combined Solubility/Mineral Trapping

It is believed that due to the time-scale of chemical reactions in brine-CO_2 systems, mineral trapping does not affect the early stages of the CO_2 sequestration process. However, small-scale precipitation may affect dissolution trapping due to the change in the dynamics of the instabilities. Precipitation and dissolution can change the porosity, which in turn can affect diffusion and the formation of fingers. In the presence of a capillary transient zone, this process will be coupled to phase behavior and become quite challenging to predict without a reliable simulation tool. Any inaccuracy in the prediction of the small-scale dissolution rate can change the predicted capacity of aquifers used for a large-scale sequestration several fold (see the example in Elenius et al., 2015). Here we present unique simulation results where the physics of all CO_2 trapping mechanisms are taken into account.

For the simulation of CO_2 fingering in the presence of chemical precipitation, the second type of small-scale model from Elenius et al. (2015) was used. In this model, the entire two-phase region was located in the high volume area, which maintains the original CO_2 profile. This model represents the leading part of the CO_2 plume. For simplicity we used the same configuration and composition of the plume as in the previous simulation, but increased the temperature to T = 380 K, which decreased the CO_2 solubility to x_{CO2} = 0.016. At conditions described in Table 6, the higher concentration of CO_2 triggers the carbonate reaction (Eq. 23), which increases the concentration of CO_2 and, in turn, initiates precipitation of $CaCO_3$ based on Eq. 22.

The influence of chemical precipitation on the generation of fingers is shown in Fig. 8. The top figures correspond to the concentration of CO_2 in brine at different simulation times. This distribution is shown for the reference case where the precipitated mineral is changing (decreasing) the porosity based on a constant mineral volume (see Appendix B) and permeability of the reservoir using the Kozeny-Carman equation. The resulting porosity changes at different times are shown in the middle row of Fig. 8. The lower row of Fig. 8 shows the absolute difference in concentrations between the reference simulation shown in the upper row and the simulation without an update in porosity and permeability.

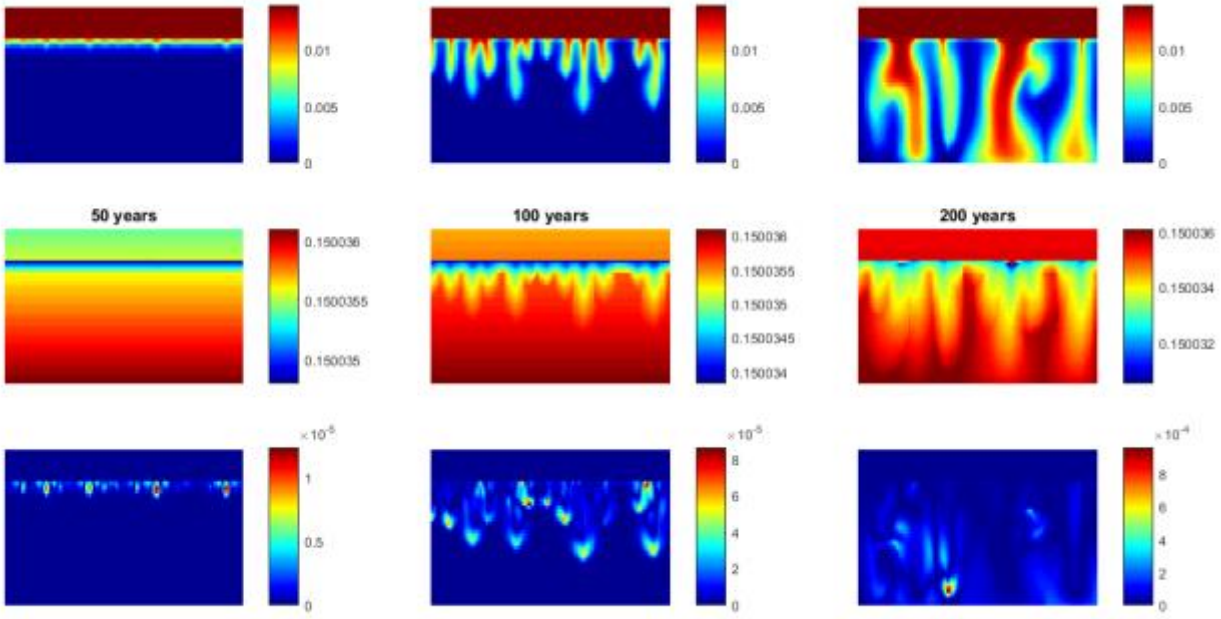

Figure 8: Small-Scale Simulation Results with $CaCO_3$ Precipitation: (upper row) overall CO_2 composition; (middle row) porosity; (lower row) difference in CO_2 composition for cases with and without porosity and permeability update.

Note that the difference in CO_2 distribution is insignificant and clearly suggests that the influence of early-time mineralization can be ignored in the accurate estimation of the CO_2 dissolution rate for the system studied. However, this does not guarantee that at different thermodynamic or chemical reaction conditions, the same conclusion will hold.

In the next simulation we keep the same system, but amplify the molar volume of minerals to update the porosity 1000 fold. It can be seen in Fig. 9 that the porosity variation in this case is more significant due to the larger pore volume occupied by minerals resulting from precipitation. In this case, the dynamics of the fingering process have changed, which affects the subsequent macroscopic dissolution rate.

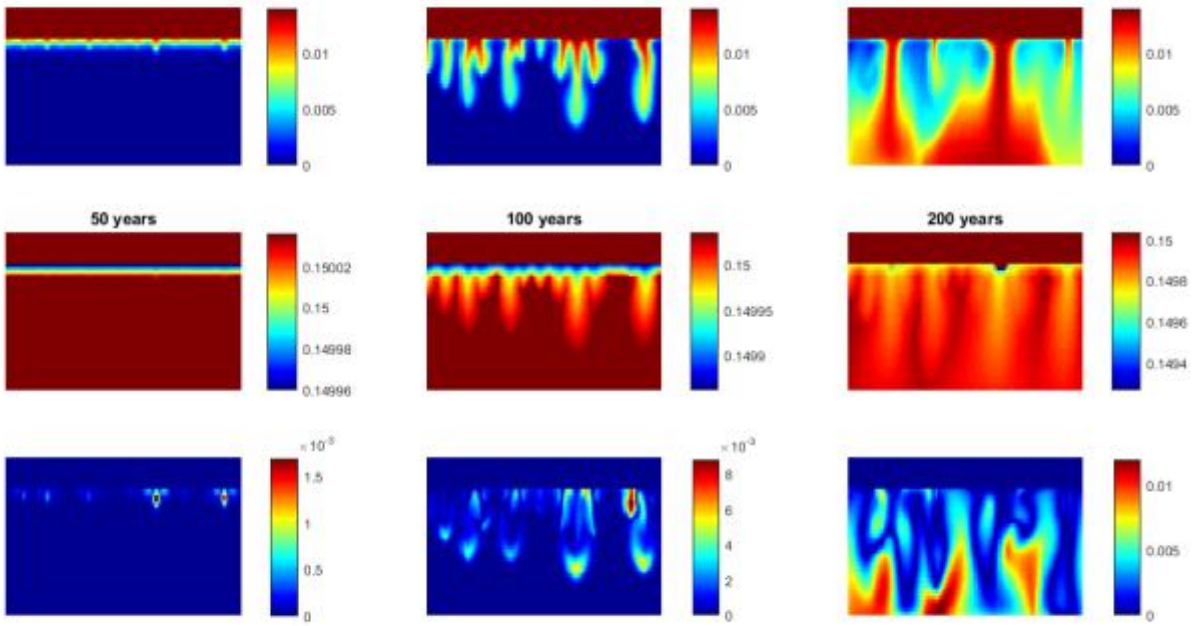

Figure 9: Small-Scale Simulation Results with $CaCO_3$ Precipitation at Magnified Molar Volume: (upper row) overall CO_2 composition; (middle row) porosity; (lower row) difference in CO_2 composition for the previous case and the case with magnified molar volume

Obviously, the last case is hypothetical since the molar volume of $CaCO_3$ for the porosity update is unrealistically large.

In the next simulation, we assume a presence of NaCl with an initial concentration C_{NaCl} = 1 kmol/m^3 and the same under-saturated brine. The dynamics of the instability completely changes in this case, and no fingers are formed in the reservoir formation. See Fig. 10. Here, the increase in porosity due to the dissolution of NaCl in the diffusion zone and the reduction of solubility due to the presence of Na^+ and Cl^- ions stabilizes the CO_2-brine interface and prevents fingers from growing.

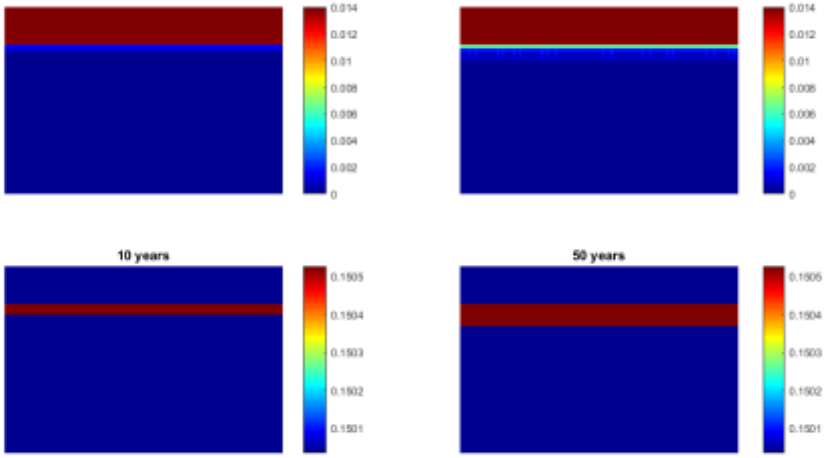

Figure 10: Small-Scale Simulation Results with CaCO3 Precipitation and NaCl Dissolution: (upper row) overall CO_2 composition; (lower row) porosity changes.

5. Conclusion

A multi-scale framework for modeling and simulating reactive transport in subsurface hydrology with fully coupled with equilibrium phase behavior of complex mixtures in homogeneous to highly heterogeneous reservoir formations was developed. The key attributes of this numerical reservoir simulation framework include the capabilities to model (1) simultaneous chemical/phase equilibrium, (2) homogeneous and heterogeneous chemical reactions, (3) aqueous electrolytes, and (4) mineral precipitation/dissolution. Simultaneous multi-component, multi-phase/chemical equilibrium was modeled using a combination of the multi-scale Gibbs-Helmholtz constrained (GHC) equations of state to describe the behavior of all fluid phases and Gibbs free energies and enthalpies of formation to predict equilibrium solubility products. Precipitation was identified using comparisons of equilibrium and ion solubility products. Governing partial differential conservation and constraint equations are solved using a fully implicit method (FIM). All modeling capabilities were implemented in the coupled software system ADGPRS/GFLASH.

Four different types of processes related to subsurface CO_2 sequestration were used to test the efficacy of the proposed framework. Using the multi-component mixture CO_2 and brine with dissolved ion Na^+, Ca^{2+}, Cl^- and CO_3^{2-}, the first example demonstrated that the modeling framework successfully predicted the formation and dissolution of solid salts NaCl and $CaCO_3$ throughout an isothermal and homogeneous reservoir formation in the presence of brine and a CO_2-rich super-critical fluid. The second example was similar to the first but also included two additional modeling challenges (1) the equilibrium reaction between CO_2 and water to form carbonate and hydronium, H_3O^+, ions and (2) vertical migration of a CO_2 plume. Therefore this example was used to demonstrate combined homogeneous/heterogeneous chemical reactions, salt dissolution, buoyancy driven flow, and simultaneous phase and chemical equilibrium. It was also shown that the carbonate chemistry resulted in insignificant changes in the

initial pH of the reservoir, which was assumed to be 11. Accordingly, pH changes were neglected in this second example. Here again, numerical results showed that the proposed framework was capable of successfully modeling all of the relevant physics. The third and fourth examples were used to demonstrate that ADGPRS/GFLASH can capture all of the higher fidelity physics of the interplay between residual, solubility, and mineral trapping in the presence of unstable CO_2 fingers, which enhance the macro-scale CO_2 solubility in brine, following buoyancy-driven flow of a CO_2 plume.

Accurate modeling of all physics in this work (i.e., rigorous, complex EOS-based simultaneous phase and chemical equilibrium involving homogeneous and heterogeneous reactions) is essential for developing a high fidelity model for carbon sequestration in any reservoir-specific environment. To our knowledge there is no software system currently available with all of these capabilities. The use of a rigorous EOS allows us to treat impurities such as O_2, Ar, SO_2, CH_4, N_2, H_2S, etc. Impurities can have strong effects on the density of the CO_2-rich phase as well as the solubility of CO_2 in the aqueous phase, which in turn can affect the migration and spread of the injected CO_2 plume and CO_2 storage capacity (Sin, 2015). Therefore, the next phase of this work will include the development of models that include impact of impurities on CO_2 sequestration.

Acknowledgements
We acknowledge financial support from the Petroleum Institute and Abu Dhabi National Oil Company. We also acknowledge the SUPRI-B program at Stanford University for permission to use ADGPRS and Sara Farshidi and Maria Elenius for helpful discussions.

Nomenclature

a	cubic EOS attractive parameter
$\mathbf{a}$	vector of mass accumulations
b	cubic EOS repulsive parameter
C	number of components
E	number of elements
$\mathbf{E}$	stoichiometric matrix
G	Gibbs free energy
H	enthalpy
$\mathbf{I}$	vector of fluxes
K	ion solubility product
p	pressure
P	number of phases
q	vector of well source terms
Q	number of reactions, equilibrium solubility product
r, $\mathbf{r}$	reaction rate, vector of reaction rates
R	ideal gas constant, number of reactions
S	saturation
T	temperature

U internal energy
x vector of mole fractions
x, y, z directions in Cartesian coordinates

Greek symbols
φ porosity
ρ density
v stoichiometric coefficients

Subscripts and superscripts

c critical property
D departure function
f formation
i component index
k phase index
L liquid state property

References

Abadpour, A., & Panfilov, M. (2009). Method of negative saturations for modeling two-phase compositional flow with oversaturated zones. *Transport in Porous Media*, *79*(2), 197–214. doi:10.1007/s11242-008-9310-0

Bachu, S., & Adams, J. J. (2003). Sequestration of CO_2 in geological media in response to climate change: capacity of deep saline aquifers to sequester CO_2 in solution. *Energy Conversion and Management*, *44*(20), 3151–3175. doi:10.1016/S0196-8904(03)00101-8

Bandura, A. V., & Lvov, S. N. (2006). The ionization constant of water over wide ranges of temperature and density. *Journal of Physical and Chemical Reference Data*, *35*(1), 15–30. doi:10.1063/1.1928231

Celia, M. a., & Nordbotten, J. M. (2009). Practical modeling approaches for geological storage of carbon dioxide. *Ground Water*, *47*(5), 627–638. doi:10.1111/j.1745-6584.2009.00590.x

Chen, C., & Song, Y. (2005). Extension of Nonrandom Two-Liquid Segment Activity Coefficient Model for Electrolytes. *Ind. Eng. Chem. Res.*, *44*(1), 8909–8921. doi:10.1021/ie049463u

Coats, K. H. (1980). An equation of state compositional model. *Society of Petroleum Engineers Journal*, *20*(05), 363-376.

Elenius, M. T., Nordbotten, J. M., & Kalisch, H. (2014). Convective mixing influenced by the capillary transition zone. *Computational Geosciences*, *18*(3-4), 417–431. doi:10.1007/s10596-014-9415-1

Elenius, M. T., Voskov, D. V., & Tchelepi, H. A. (2015). Interactions between gravity currents and convective dissolution. *Advances in Water Resources*, *83*, 77–88. doi:10.1016/j.advwatres.2015.05.006

Farshidi, S. (2016). Compositional reservoir simulation-based reactive-transport formulations, with application to CO_2 storage in sandstone and ultramafic formations. PhD Thesis, Stanford University.

Flemisch, B., Darcis, M., Erbertseder, K., Faigle, B., Lauser, A., Mosthaf, K., … Helmig, R. (2011). DuMux: DUNE for multi-{phase,component,scale,physics,...} flow and transport in porous media. *Advances in Water Resources*, *34*(9), 1102–1112. doi:10.1016/j.advwatres.2011.03.007

Gasda, S., Nordbotten, J. and Celia, M. (2011) Vertically averaged approaches for CO_2 migration with solubility trapping. Water Resources Research, 47(5).

Gharbia, I. B., Flauraud, E., & Michel, A. (2015, February). Study of compositional multi-phase flow formulations with cubic eos. In *SPE Reservoir Simulation Symposium*. Society of Petroleum Engineers.

Harris, J. G., & Yung, K. H. (1995). Carbon Dioxide ’s Liquid-Vapor Coexistence Curve and Critical Properties As Predicted by a Simple Molecular Model. *Journal of Physical Chemistry*, *99*, 12021–12024.

Horn, H. W., Swope, W. C., Pitera, J. W., Madura, J. D., Dick, T. J., Hura, G. L., & Head-Gordon, T. (2004). Development of an improved four-site water model for biomolecular simulations: TIP4P-Ew. *The Journal of Chemical Physics*, *120*(20), 9665–78. doi:10.1063/1.1683075

Huang, S. H., & Radosz, M. (1990). Equation of state for small, large, polydisperse and associating molecules. *Ind. Eng. Chem. Res.*, *29*, 2284–2294. doi:10.1021/ie00107a014

Iranshahr, a., Voskov, D., & Tchelepi, H. A. (2010). Generalized negative-flash method for multiphase multicomponent systems. *Fluid Phase Equilibria*, *299*(2), 272–284. doi:10.1016/j.fluid.2010.09.022

Iranshahr, A., Voskov, D.V., Tchelepi, H.A. (2013). Tie-simplex based compositional space parameterization: Continuity and generalization to multiphase systems. *AIChE J. 59* (5), pp. 1684-1701. doi:10.1002/aic.13919

Joung, I. S., & Cheatham, T. E. (2008). Determination of alkali and halide monovalent ion parameters for use in explicitly solvated biomolecular simulations. *The Journal of Physical Chemistry. B*, *112*(30), 9020–41. doi:10.1021/jp8001614

Kaszuba, J. P., Janecky, D. R., & Snow, M. G. (2003). Carbon dioxide reaction processes in a model brine aquifer at 200 °C and 200 bars: implications for geologic sequestration of carbon. *Applied Geochemistry*, *18*(7), 1065–1080. doi:10.1016/S0883-2927(02)00239-1

Kiepe, J., Horstmann, S., Fischer, K., & Gmehling, J. (2004). Application of the PSRK model for systems containing strong electrolytes. *Industrial & Engineering Chemistry Research*, *43*(1), 6607–6615.

Kim, J., Tchelepi, H. A., & Juanes, R. (2009). Stability , Accuracy and efficiency of sequential methods for coupled flow and geomechanics. *Society of Petroleum Engineers*.

Koneshan, S., Rasaiah, J. C., Lynden-Bell, R. M., & Lee, S. H. (1998). Solvent Structure, Dynamics, and Ion Mobility in Aqueous Solutions at 25 °C. *The Journal of Physical Chemistry B*, *102*(98), 4193–4204. doi:10.1021/jp980642x

Kontogeorgis, G. M., Voutsas, E. C., Yakoumis, I. V., & Tassios, D. P. (1996). An equation of state for associating fluids. *Industrial & Engineering Chemistry Research*, *35*(11), 4310–4318. doi:10.1021/ie9600203

Lagasca, J. (2014) Simulation of large-scale CO_2 plumes in deep saline aquifer. MSc Thesis, Stanford

Lauser, A., Hager, C., Helmig, R., & Wohlmuth, B. (2011). A new approach for phase transitions in miscible multi-phase flow in porous media. *Advances in Water Resources*, *34*(8), 957–966. doi:10.1016/j.advwatres.2011.04.021

Lichtner, P. C. (1985). Continuum model for simultaneous chemical reactions and mass transport in hydrothermal systems. *Geochimica et Cosmochimica Acta*, *49*(3), 779–800. doi:10.1016/0016-7037(85)90172-3

Lucia, A. (2010). A multiscale Gibbs-Helmholtz Constrained cubic equation of state. *Journal of Thermodynamics*, *2010*, 1–10. doi:10.1155/2010/238365

Lucia, A., Bonk, B.M., Waterman, R.R., Roy, A. (2012). A multi-scale framework for multi-phase equilibrium flash. *Comput. Chem. Engng. 36*, 79-98.

Lucia, A., Henley, H., & Thomas, E. (2014). Multiphase equilibrium flash with salt precipitation in systems with multiple salts. *Chemical Engineering Research and Design*, *93*(May), 662–674. doi:10.1016/j.cherd.2014.04.034

Leung, D. Y. C., Caramanna, G., & Maroto-Valer, M. M. (2014). An overview of current status of carbon dioxide capture and storage technologies. *Renewable and Sustainable Energy Reviews*, *39*, 426–443. doi:10.1016/j.rser.2014.07.093

Marchand, E. and Knabner, P. (2014). Results of the MoMas benchmark for gas phase appearance and disappearance using generalized MHFE. *Advances in Water Resources 73*, 74-96.

Martin, M. G. (2013). MCCCS Towhee: a tool for Monte Carlo molecular simulation. *Molecular Simulation*, *39*(14-15), 1212–1222. doi:10.1080/08927022.2013.828208

Maribo-Mogensen, B., Thomsen, K., & Kontogeorgis, G. M. (2015). An electrolyte CPA equation of state for mixed solvent electrolytes. *AIChE Journal*, *61*(9), 2933–2950. doi:10.1002/aic.14829

Peng, D.-Y., & Robinson, D. B. (1976). A new two-constant equation of state. *Industrial & Engineering Chemistry Fundamentals*, *15*(1), 59–64. doi:10.1021/i160057a011

Pitzer, K. S. (1977). Electrolyte theory-improvements since Debye and Huckel. *Accounts of Chemical Research*, *10*(11), 371–377. doi:10.1021/ar50118a004

Pruess, K., & Spycher, N. (2007). ECO2N a fluid property module for the TOUGH2 code for studies of CO_2 storage in saline aquifers. Energy Conservation and Management 48(6), 1761-1767.

Redlich, O., & Kwong, J. N. S. (1949). On the thermodynamics of solutions. V. An equation of state. Fugacities of gaseous solutions. *Chemical Reviews*, *44*(1), 233–244.

Sin, Irina. (2015) Numerical simulation of compressible two-phase flow and reactive transport in porous media – Applications to the study of CO_2 storage and natural gas reservoir. *PhD Thesis, ParisTech.*

Soave, G. (1972). Equilibrium Constants from a modified Redlich-Kwong equation of state. *Chemical Engineering Science*, *27*(6), 1197–1203.

Soong, Y., Goodman, A. L., McCarthy-Jones, J. R., & Baltrus, J. P. (2004). Experimental and simulation studies on mineral trapping of CO_2 with brine. *Energy Conversion and Management*, *45*(11-12), 1845–1859. doi:10.1016/j.enconman.2003.09.029

Steefel, C., Depaolo, D., & Lichtner, P. (2005). Reactive transport modeling: An essential tool and a new research approach for the Earth sciences. *Earth and Planetary Science Letters*, *240*(3-4), 539–558. doi:10.1016/j.epsl.2005.09.017

Tchelepi, H., & Zhou, Y. (2013). Multi-GPU parallelization of nested factorization for solving large linear systems. In proceeding: SPE Reservoir Simulation Symposium. doi:10.2118/163588-MS

Van Der Zwaan, B., & Smekens, K. (2009). CO_2 capture and storage with leakage in an energy-climate model. *Environmental Modeling and Assessment*, *14*(2), 135–148. doi:10.1007/s10666-007-9125-3

Voskov, D., Zaydullin, R., & Lucia, A. (2016). Heavy oil recovery efficiency using SAGD, SAGD with propane co-injection and STRIP-SAGD. *Computers & Chemical Engineering*, *88*, 115–125. doi:10.1016/j.compchemeng.2016.02.010

Voskov, D. V., & Tchelepi, H. A. (2012). Comparison of nonlinear formulations for two-phase multi-component EoS based simulation. *Journal of Petroleum Science and Engineering*, *82-83*, 101–111. doi:10.1016/j.petrol.2011.10.012

Voskov, D.V. (2011). An extended natural variable formulation for compositional simulation based on tie-line parameterization, Transport in Porous Media, 92(3), 541-557. doi:10.1007/s11242-011-9919-2

Xu, T., Apps, J. A., & Pruess, K. (2005). Mineral sequestration of carbon dioxide in a sandstone-shale system. *Chemical Geology*, *217*(3-4), 295–318. doi:10.1016/j.chemgeo.2004.12.015

Xu, T., Spycher, N., Sonnenthal, E., Zhang, G., Zheng, L., & Pruess, K. (2011). Tough react version 2.0: A simulator for subsurface reactive transport under non-isothermal multiphase flow conditions. *Computers and Geosciences*, *37*(6), 763–774. doi:10.1016/j.cageo.2010.10.007

Zaydullin, R., Voskov, D., & Tchelepi, H. A. (2012). Nonlinear formulation based on an equation-of-state free method for compositional flow simulation. Society of Petroleum Engineers. doi:10.2118/146989-PA

Zaydullin, R., Voskov, D. V., James, S. C., Henley, H., & Lucia, A. (2014). Fully compositional and thermal reservoir simulation. *Computers & Chemical Engineering*, *63*, 51–65. doi:10.1016/j.compchemeng.2013.12.008

Zeebe, R. E. (2011). On the molecular diffusion coefficients of dissolved CO_2, HCO_3^-, and CO_3^{2-} and their dependence on isotopic mass. *Geochimica et Cosmochimica Acta*, *75*(9), 2483–2498. doi:10.1016/j.gca.2011.02.010

Appendix A: pH Change Due to $CaCO_3$ Formation

Let the pH of the brine solution be 11. It is demonstrated that the amount of hydronium ion produced is small so that associated changes in pH can be neglected.

The maximum $CaCO_3$ concentration obtained in examples in this work was ~$1.3\text{x}10^{-3}$ mol/L. From reactions (5 and 6), the concentration of hydronium ion corresponding to this amount of $CaCO_3$ is $[H_3O^+]$ = $2.6\text{x}10^{-3}$ mol/L. Also, the equilibrium constant for the dissociation of water into hydronium and hydroxide ions at 350 K and 250 bar using linear interpolation is $K_w = 1\text{x}10^{-12.58}$ (see, Bandura et al., 2006).

At a pH of 11, the initial hydroxide concentration is

$$[OH^-] = \frac{K_w}{[H_3O^+]} = 0.0263\,\frac{mol}{L} \qquad \text{(A1)}$$

Hydronium ions from the reaction between CO_2 and water react with hydroxide ions, resulting in a change in hydroxide concentration given by

$$[OH^-] = 0.0263 - 2.6x10^{-3} = 0.0237\,\frac{mol}{L} \quad \text{(A2)}$$

Finally, the new equilibrium hydronium ion concentration is

$$[H_3O^+] = \frac{K_w}{[OH^-]} = \ 1.11\ x\ 10^{-11} \quad \text{(A3)}$$

which corresponds to a pH of 10.95.

Therefore, for the examples studied in this article, the amount of hydronium ion produced as carbonate ion is formed does not significantly change the pH of the formation brine.

Appendix B: Fluid and Rock Properties

Table B.1: Critical properties

Component	T_c (K)	P_c (bar)	b_{GHC}(cm^3bar/mol)
CO_2	304.20	73.80	28.169
H_2O	647.37	221.20	16.363

Table B.2: Enthalpy and Gibbs free energy of formation data

Component	ΔH_f(kJ/mol)	ΔG_f(kJ/mol)
NaCl	-411.2	-384.1
$CaCl_2$	-795.8	-748.1
Na_2CO_3	-11130.7	-1044.4
$CaCO_3$	-1206.9	-1128.8

Table B.3 – References for Monte Carlo simulation potential parameters

Component	Reference
H_2O	Horn et al., 2004
CO_2	Harris and Yung, 1995
Na^+	Yung and Cheatham, 2008
Ca^{2+}	Koneshanet al., 1998
Cl^-	Yung and Cheatham, 2008
CO_3^{2-}	Zeebe, 2011

A Corey-type relative permeability model was used to define the relative permeability as a function of saturation (Eqs. B1-B3), the parameters are given in Table B.4.

$$S_{pe} = \frac{S_p - S_{pr}}{1 - S_{pr} - S_{or}} \quad \text{(B1)}$$

$$k_{pr} = \left(S_{pe}\right)^{n_p} \quad \text{(B2)}$$

$$k_{or} = \left(1 - S_{pe}\right)^{n_o} \quad \text{(B3)}$$

In the third example, the residual water and CO_2 saturations were each set to 0.2, and the relative permeability and saturation distribution were determined by specifying a static pressure distribution in each phase (see Elenius et al., 2015) to create a capillary transition zone at the interface between the two phases.

Table B.4: Additional Parameters

	Parameter	Value	Description
Common for all examples	C_r	1.0e-06 1/bar	rock compressibility
	N_p	2	aqueous phase exponent
	N_o	2	CO_2-rich phase exponent
Example #1	S_{pr}	0.0	aqueous phase residual saturation
	S_{or}	0.0	CO_2-rich phase residual saturation
Examples #2 to #4	S_{pr}	0.2	aqueous phase residual saturation
	S_{or}	0.2	CO_2-rich phase residual saturation

The viscosities of the brine phase and the CO_2-rich phase were assumed to be constant in all examples in this work. Values of 0.511 and 0.061 cP were chosen for the brine and CO_2 phases, respectively, based on values used in a similar study (Elenius et al., 2015).

Figure Captions

Figure 2: Schematic Diagram Illustrating Information Flow in ADGPRS/GFLASH Framework

Figure 2: CO_2-rich Phase Saturation Distribution

Figure 3: Equilibrium Phase State Distribution

Figure 4: CO_2 Rich Phase Saturation Distribution

Figure 5: Distribution of CO_2 Mole Fraction in the Brine Phase

Figure 6: Distribution of Precipitated $CaCO_3$ ($kmol/m^3$)

Figure 7: Distribution of CO_2 in Brine at Different Times and Macroscopic Dissolution Rate of CO_2 as a Function of Time for Simulation at T = 345 K

Figure 8: Small-Scale Simulation Results with $CaCO_3$ Precipitation:
(upper row) overall CO_2 composition; (middle row) porosity changes;
(lower row) difference in CO_2 composition for cases with and without porosity and permeability update

Figure 9: Small-Scale Simulation Results with $CaCO_3$ Precipitation at Magnified Molar Volume:
(upper row) overall CO_2 composition; (middle row) porosity changes;
(lower row) difference in CO_2 composition for the previous case and the case with magnified molar volume

Figure 10: Small-Scale Simulation Results with $CaCO_3$ Precipitation and NaCl Dissolution:
(upper row) overall CO_2 composition; (lower row) porosity changes